A Battery Model for Transportation and Stationary Applications

E. Dahlquist* M. Azaza* M. Shabani***

J. R. Vazquez M. M. Nezhad*** A. Fattouh**** A. D. Fentaye***

**Mälardalen University (MDU), School of Business, Society and Engineering, Future Energy Center, Universitetsplan 1, 72123 Västerås, Sweden (e-mail: erik.dahlquist@mdu.se, maher.azaza@mdu.se, amare.desalegn.fentaye@mdu.se)*

***Hitachi Energy, Valhallavägen, 77131 Ludvika, Sweden (e-mail: josefin.rojas.vazquez@hitachi.se)*

**** Mälardalen University (MDU), Department of Sustainable Energy Systems, Universitetsplan 1, 72123 Västerås, Sweden (e-mail: meysam.majidi.nezhad@mdu.se)*

***** Mälardalen University (MDU), School of Innovation, Design and Technology (IDT), Division of Product Realization (PR),63105 Eskilstuna, Sweden (e-mail: anas.fattouh@mdu.se)*

Abstract: Batteries are used in electric vehicles as well as in stationary applications. In electric vehicles, high energy density, as kilowatt hour per kilogram (kWh/kg), is needed while stationary applications are less sensitive to the energy density. Principally, it may be a good idea first to use batteries for transportation applications and then when capacity has reached a certain level start using them for other applications in a "second life". Both for optimizing the performance of operations in 1st and 2nd life and for making fair commercial agreements when selling used batteries for second life applications, there is a need to make predictions of Remaining Useful Life (RUL) and State of Health (SoH). For this purpose, battery models are needed. This paper presents a methodology for building a useful battery model based on our experiments and literature data. Single cells and cells in series of Nickel Manganese Cobalt (NMC) batteries and Lithium Iron Phosphate (LFP) batteries have been cycled. Electrochemical Impedance Spectra (EIS) and differential capacity (dQ/dV) have been measured for each cycle. These data were then used to develop SoH and RUL models using various regression methods. The developed models are described and discussed, and the results are presented in the paper.

Keywords: Battery model, electric vehicles (EV), stationary applications, kilowatt hour per kilogram (kWh/kg), Nickel Manganese Cobalt (NMC), Lithium Iron Phosphate (LFP), Electrochemical Impedance Spectra (EIS), differential capacity (dQ/dV), regression.

1. INTRODUCTION AND RELATED WORK

There is a strong interest in following the degradation of batteries during the first life to give the possibility to predict the remaining useful life (RUL) for the battery, especially for the second-life use of batteries. By following the state of health (SoH) continuously, correlating it to how the battery has been used, and following it until it is totally wared out, reasonably good prediction models can be determined and used. This information can be utilized for 2nd life use of batteries (Chirumalla et al., 2023, 2024).

In this paper, we want to extract experience from what has been done earlier and add to it our own battery modeling approach for the simulation of batteries used in Vehicles. For second life use of batteries there is a high interest to use for power grid balances as shown in e.g. Dahlquist et al. (2023).

Many researchers have modelled battery performance in different ways. Pelletier et al. (2017) focused on modelling cycle-life as a function to the depth of discharge (DOD) and discharged rate relative to the battery maximum capacity (C-rate). Ahmadiana et al. (2018) modeled battery resistance growth versus state of charge (SoC) and battery degradation as a function to DOD. Maheshwari et al. (2020) have modelled cycling life vs C-rate using a non-linear model. O'Kane et al. (2022) have used the PyBaMM, an open source modelling environment for simulation of the effect of different variables important for degradation of Li-ion batteries. Four degradation mechanisms are coupled in PyBaMM. The most important ones are the loss of lithium inventory and the loss of active material. For the same cell, five different pathways have been evaluated. Lam and Bauer (2012) performed a lot of cycling of LFP batteries and from the experiments, an empirical model was constructed, which was capable of modeling the capacity fading in electric vehicles (EV) battery cells under most operating conditions. Ravali and Raju (2023) developed a Lithium-Ion Battery model for estimation of degradation capacity and SoC using Sigma Point Kalman filter. After one thousand cycles, the amount of capacity faded from 24Ah to 20.5Ah at 25°C.

de la Vega et al. (2023) have proposed to monitor battery performance by measuring instantaneous terminal cell voltage as a function to SoC during the first discharge cycle, as a reference cycle, and the n^{th} cycle. The SoC interval [SoC_{min}, SoC_{max}] = [0.55, 0.75] was chosen to calculate the ΔVRMS indicator, which is terminal voltage difference between first and n^{th} cycle at SoC_{min} and SoC_{max}. This is an interesting

approach to give the possibility to follow the degradation continuously if the values at SoC_{min} and SoC_{max} are stored continuously.

Shamarova et al. (2022) have developed a method utilizing data from electrical circuit models (ECM) where dependency of ECM parameters on the electrochemical properties of the battery was examined in using a pseudo-two-dimensional (P2D) model. This is combining physical and statistical modelling approaches. Wildfeuer et al. (2023) made a set of experiments studying impact on SoH for capacity, resistance, Li-inventory, positive electrode losses, and negative electrode losses for SoC 10-100% and temp 20-60ºC for NAC batteries. Panchal et al. (2017) did similar experimental studies for LFP batteries.

Drive cycles with different modes like acceleration, constant speed, and deceleration in both highway and city driving were implemented at −6°C, 2°C, 10°C, and 23°C ambient temperatures with all accessories on. 4.6% capacity fade occurred over 3 months of driving. The empirical degradation model was fitted to these data, and an extrapolation estimated that 20% capacity fade would occur after nine hundred daily drive cycles. This is a high degradation rate, but experimental data and model were close for the 3 months test period. Zhang et al. (2023) have compared LFP and NMC batteries. Degradation characteristics during charging of LiFePO4 (LFP)/Graphite batteries at voltages of 3.65–4.8V and Li(Ni0.5Co0.2Mn0.3)O2 (NCM)/Graphite batteries at 4.2–4.8V at −10 °C with currents of 0.2–1A were determined. The loss of active material (LAM) causes the height of the highest IC peak (dQ/dV-V) to decrease for a given voltage, while the loss of Lithium inventory (LLI) shifts the DV curve (dV/dQ-Q) toward lower capacities.

It can also be interesting to see what measurements on real vehicles indicate with respect to capacity losses. Salazar and Bengoechea (2021) have summarized information reported by different Tesla Model 3 owners. One had a decrease of capacity by 4.8% during 136,000km operation, another 2.3% loss during 22,000km, when the vehicle was charged to 10% five days a week. A third had a 2.2% decrease during 32,000km of SoH for 12 months operation. In this case all the cars had LFP batteries.

Shen et al. (2019) tried to make RUL predictions. They were working with NASA data set and the CALCE data set. They compared their own model to another approach. Still, the value is to use common data sets for comparing different modelling approaches. Uddin et al. (2016) used an approach with identification and tracking of electrochemical battery model Parameters. This combines physical and statistical methods. The method was demonstrated on a 3.03Ah LiC6/NCA battery stored at 45°C with 50% SoC for 476 days.

Rahbari et al. (2018) used another approach with an Adaptive Neuro-Fuzzy Inference System for SoH of real-life plug-in hybrid electric vehicles (PHEVs). The model was representing the experimental data in a good way. Dai et al. (2018) showed a SoH estimation method by using prior knowledge-based neural network (PKNN) and Markov chain for a single lithium-ion battery. Shi et al. (2019) used another method with estimation of the state of health (SoH) for a lithium-ion battery based on the ohm internal resistance R0. They were considering the variation of R0 with the state of charge (SoC), which was new.

This overview covers a broad spectrum of methods, although many other techniques are also utilized. From all this, we developed a simplified battery degradation model that can be adapted to different types of batteries and with reasonable values for impact of different variables like temperature, C-rate, DOD/DOC and calendric time.

The paper is organized as follows. Section 2 presents the experiment setup while Section 3 presents the experimental data, both our data and other data from literature. In Sections 4 and 5, we develop a battery degradation model and power demand model from vehicle, respectively. The paper ends with discussion and conclusions in Section 6.

2. EXPERIMENTS SETUP

2.1 Testing of battery cells

Single cells can be tested with Electrochemical Impedance Spectroscopy (EIS). The spectra are made by measuring the current and the capacity as a function of voltage as the frequency of the supplied current is going from 1000Hz to 0.001Hz. At high frequencies, we see the resistance in the electrolyte, at mid frequencies capacitance over the electrode surface, and at low frequencies the inner resistance of the cells as such. By following the EIS at the start and after a number of cycles, you can get both a quantitative measure of the overall degradation over time as well as an indication of what mechanisms in the battery cells are causing this.

Another measure is to follow dQ/dV or dV/dQ, as a function of V, where Q is cell capacity (Ah) and V voltage. By measuring and plotting this over cell cycles a battery performance pattern is achieved. This can be measured continuously during the use of the cell, which is not possible with the EIS, and thus can be a good complement. Figure 1 depicts a system for prediction of RUL, SoH and SoC.

There is a correlation between DoD (depth of discharge)/DoC (depth of charge) and degradation rate. Figure 2 shows this correlation presented by Qadrdan et al. (2018). Real operation with Tesla cars still indicates that this curve is not relevant for NAC batteries in “real life” operations.

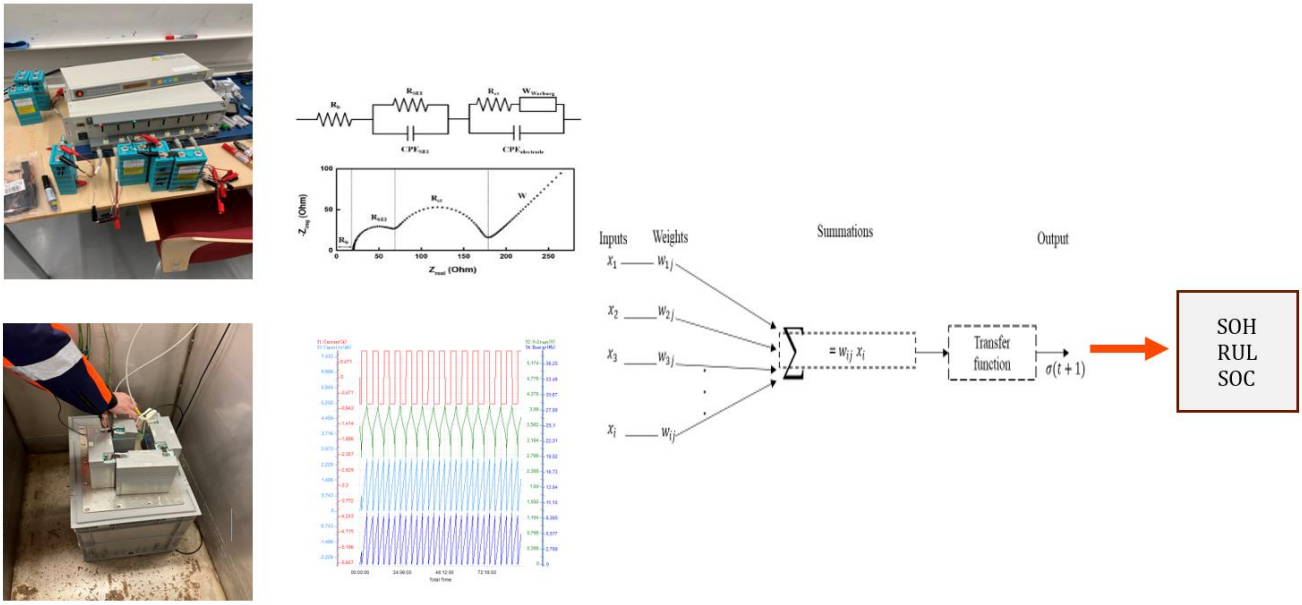

Fig. 1. Experimental setup to collect data that will be used to develop algorithms for prediction of SoH, RUL, and SoC.

$$DoD = removed\ amount\ of\ charge / maximum\ available\ amount\ of\ charge = Qd/C * 100\ [\%]$$

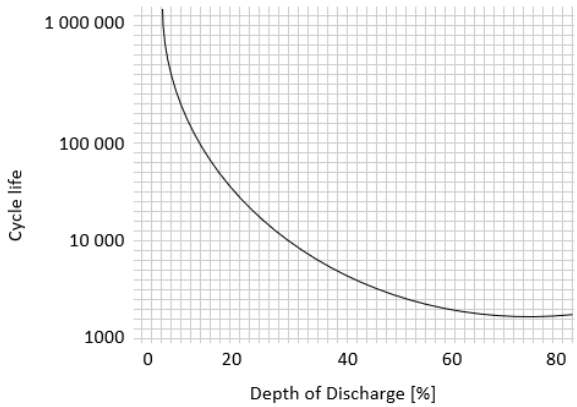

Fig. 2. Battery cycle life as a function to depth of discharge. Adapted from Qadrdan et al. (2018).

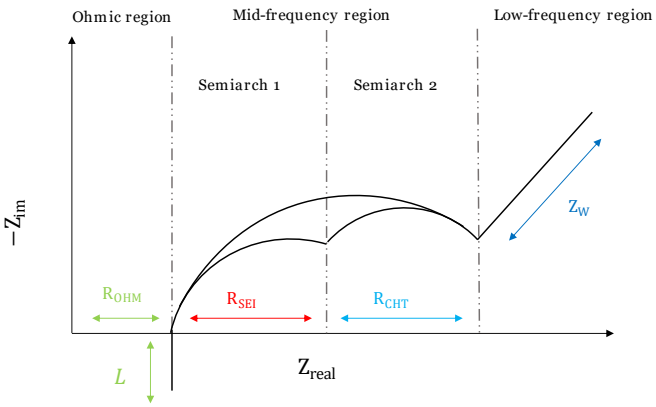

Fig. 3. Analysis of EIS in a Nyquist plot inspired by Li et al. (2020), and Iurilli et al. (2021).

The SoH can be shown in an EIS, Electrochemical impedance spectrum. In Fig. 3, we see how the pattern in a Z_{real} vs Z_{im} is looking like when a frequency scan is made from 1000Hz to 0.001Hz. Higher frequency is to the right. Closest to y-axis we have ohmic resistance (Rohm):

$$\begin{aligned} Z(\omega) &= \tilde{V}(\omega)\tilde{i}(\omega) \\ &= |\tilde{V}(\omega)\tilde{i}(\omega)|(\cos\phi(\omega) + j\sin\phi(\omega)) \\ &= Zr + jZj \end{aligned}$$

The impedance spectrum can also be represented as an equivalent electric circuit model as shown in Fig. 4.

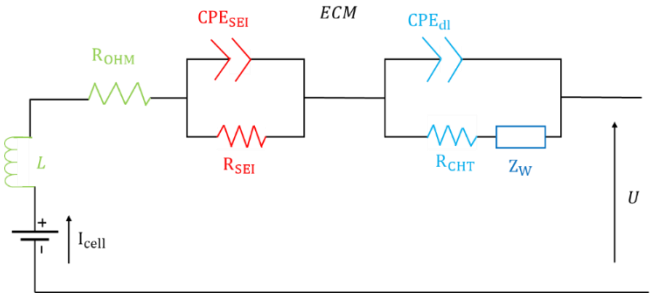

Fig. 4. Common equivalent circuit model inspired by Xiong et al. (2020).

According to Xiong et al. (2020), the model in Fig. 4 is the most common ECM, which is composed of three parts:

- Part 1: a series of R_{OHM} and L.
- Part 2: a parallel of CPE_{SEI} and R_{SEI}.
- Part 3: a parallel of CPE_{dl} and series of R_{CHT} and Z_W

Part 1 indicates the ohmic resistance increase, where R_{OHM} incorporates the ohmic resistance of electrolytes, electrode, binder and current collector. It can be acquired by resolving the intersection among the impedance spectrum and high frequency region of the Nyquist plot. The inductance incorporated the high frequency phenomena occurring in the collector, can be acquired by the impedance positive imaginary part. Part 2 describes the formation, decomposition and growth of SEI film, where the R_{SEI} is calculated from the first semi arch span at mid-frequency. Part 3, R_{CHT} the charge transfer resistance attained by a second semiarch at low frequency, CPE_{dl} simulates the double-layer affect that occurs during battery discharge for the shape of electrode according to Xiong et al. (2020).

In our cycling tests we have collected spectra with dQ/dV as a function of voltage and number of cycles. Here we can see how the spectrum for the same battery is changing pattern. In this case we cycled NMC batteries model 18650 up to four hundred cycles from 3.3 to 4.2 Volt. The results are shown in Fig. 5.

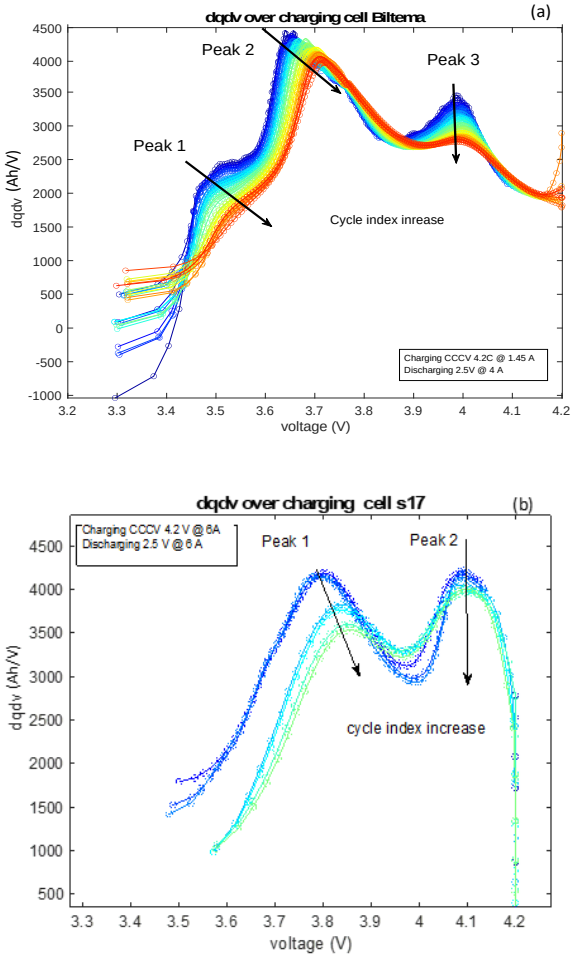

Fig. 5. Results of the incremental capacity analysis over the cell's cycling (a) NMC cell from Biltema and (b) NMC cell from Samsung.

The shift in pattern during cycling is shown as a few arrows. This information can be used to predict the performance of the batteries. It can also be used for prediction of remaining useful life, RUL, if cycling proceeds until the capacity has faded to below 70-80% of the original SoH.

In Fig. 6, we see how the EIS changes during cycling. The diagram to the left is for fresh batteries while the others are after several cycles. The higher the cycle number, the further to the right.

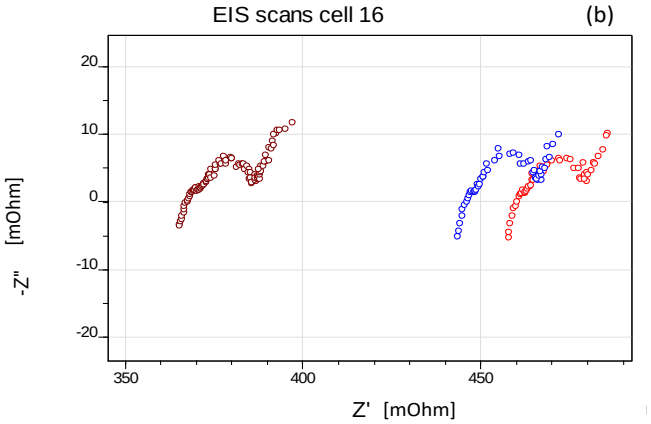

Fig. 6. Electrochemical impedance spectra (EIS) for a NMC battery from Samsung after Nyquist plot for battery cell (marked 16): cycle 200, 207 and 300. Experiments performed at MDU.

From experimental data, regressions and prediction models have been developed using different AI-algorithms. Results from these are exemplified in Fig. 7.

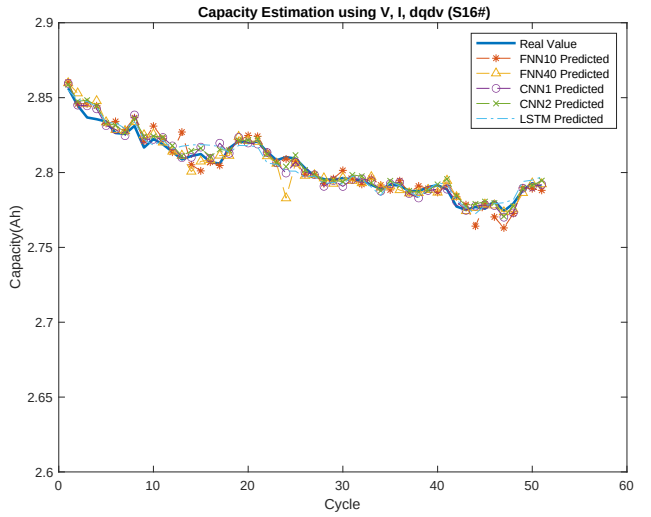

Fig. 7. Battery capacity estimation using different deep-learning algorithms as a function of cycle number (FNN10,FNN40,CNN1,CNN2 and LSTM). Rojas Vazquez (2023).

Some other approaches using different type of models is e.g. capacity degradation estimation using sigma point Kalman filter (Gaddipati and Kuthuri, 2023) and Lin et al (2023) using a data driven approach.

2.2 Testing of battery packs

For many cells in series and parallel, it is difficult to perform EIS, while dQ/dV or dV/dQ is possible to measure. By comparing this for packs as well as single cells, and

performing EIS as well for the single cells, we can create data that can be used to make AI models for different types of performance numbers. These can be state of charge (SoC), state of health (SoH), remaining useful life (RUL), and similar. By measuring full cycles for batteries and packs when fresh and after different numbers of cycles, prediction models can be developed. Also the depth of discharge (DoD), that is how close to 0% charge you go, is of interest to monitor. C-rate for both charge and discharge as well as temperature in the cell packs are other factors.

3. EXPERIMENTAL DATA

3.1 Our experimental data

Previously we presented data from NMC battery cycling performed at our lab. We also have done testing with LFP batteries, or more correct Lithium Iron Manganese Phosphate batteries with 20Ah capacity. The latter are prismatic, while the first ones are cylindrical with a 2.9Ah capacity.

As seen above, the degradation during fifty cycles of a NMC battery was 1.8% or 0.035% per cycle, when cycling between 2.5V and 4.2V. Another cell was cycled 325 cycles between 2.5V and 4.2V with 1.5A charging current (C-rate= 0.52) and 3A discharge current (C-rate =1.04). The decrease in capacity went from 2.91Ah to 2.73Ah, or 0.18Ah. This means 6.2% during 325 cycles or a decrease of 0.019% per cycle. If we just look at the first fifty cycles of the same battery (S20), the decrease was from 2.91Ah to 2.81Ah, or 3.4%, or 0.069% per cycle. There is a faster degradation in the beginning, but it is reduced with time.

For the LFP batteries, we had a degradation of 0.12% per cycle at C-rate 0.15 during thirty-nine cycles, when cycling between 2.5V and 3.7V at 3A for the 20Ah batteries. It was the same for charging and discharging.

We did the same cycle for LFP batteries but with four cells in series with 10A and 40A respectively. This corresponds to a C-rate of 0.5 and 2 respectively. For the reference case with C-rate 0.5 and cycling only between 12.6V to 13.7V for four batteries, corresponding to 3.15-3.4V per cell. We could not see any degradation at all after one hundred cycles with this mild cycling. For C-rate 2, 40A, we saw a small degradation by 0.0079% per cycle during 102 cycles. When running at C-rate 0.5, the temperature increase was around 2-3ºC but for C-rate two it was 55-65ºC measuring between the cells at various positions. The lower temperature was at the entrance and outlet from the series, while the higher temperature was between the cells.

A problem with these measurements is that we get slightly non-linear degradation. The degradation is higher in the first fifty cycles compared to later. This also will depend on temperature, C-rate, and other factors. To get more insights, we have collected data from the literature as explained in the next subsection.

3.2 Other experimental data

Tests with different Tesla cars with NAC batteries were made with fast charging 90% of the time (Tesla 3 and Tesla Y) and compared to Tesla models with only 10% fast charging. This was followed 1000- 2000 days. What they found was that the degradation was very similar in both cases (SOH from 99% to 91% for 1000 days and 89% for 2000 days. The % is the percent of the SOH measured as original distance with fully charged batteries after use compared to fresh batteries). Still, here the temperature control has been good, and a charging pattern with low power close to full charge (around 80-90%). Still, it is not known how degradation affects the long-term capacity like 10-20 years.

Later the Tesla user's organization compared LFP batteries. Salazar and Bengoechea (2021) have summarized information reported by different Tesla Model 3 owners, who have LFP batteries. One had a decrease of capacity by 4.8% during 136,000 km operation; another 2.3% loss during 22,000 km, when the vehicle was charged to 100% five days a week. A third had 2.2% decrease in SOH during 32,000 km and 12 months of operation. In this case, all the cars had LFP batteries. The second Tesla owner says he was charging to 100% five days a week, which is higher DOC than recommended. Also, the others said they often charged to 100%. A Tesla model 3 consumes 1.4-1.7kWh/10km which means 136,000 km corresponds to some 19,000 – 23,100kWh total charging. The battery capacity is some 55-77kWh depending on the model, so it corresponds to 250- 420 full battery cycles. 4.8% total degradation then corresponds to 0.011-0.019% per cycle. The second had a loss of 2.3% during 2,000 km or 3080–3740kWh. This means forty -68 full cycles, or 0.058- 0.034% per cycle.

Zhang et al. (2023) studied the degradation of both LFP and NMC batteries as a function of temperature and C-rate. The LFP batteries were charged to 3.65V while the NMC batteries were charged to 4.2V. The degradation is seen in Table 1.

Table 1. Degradation of LFP and NMC batteries as a function of C-rate and Temperature according to Zhang et al. (2023)

	% degradation per cycle					
C-rate	0.2		0.5		1	
Temp	25ºC	-10ºC	25ºC	-10ºC	25ºC	-10ºC
NMC	0.02		0.07		0.05	
NMC			0.0375	1.16	0.4125	3.6
LFP	0.03		0.25		0.36	
LFP			0.0233	0.26		

Lin et al. (2023) have studied SoH in relation to internal resistance. They found a degradation of SoH by 8% during three hundred cycles while the inner resistance increased from 0.18 to 0.213 Ohm. The SoH decrease per cycle was 0.027%.

Shabani et al. (2023) have shown that DOD/DOC has an impact on degradation, but also where in the span charge and discharge occur. With the same total cycle depth but with different spans you see different degradation. With DOC =50%, we can see that the degradation rate goes from 12 to

14.5% for 10 years when having a cycle of 40-90% SoC compared to 10-60% SoC. When we increase the DOC above this span of 50%, we also see an increased fade. How much this is depends on temperature, battery type, and C-rate?

3.3 Summary of degradation data

If we try to summarize the data, both our own and others' data, we get a high variation as % per cycle, but still, we can see some trends. An increased C-rate above 0.5-1 usually increases the fade of SoH. When the temperature is below 0-10ºC and above 30ºC, we also see an increased degradation rate. The difference between LFP and NMC batteries is not clear from these data. What can be seen is that the value for the same condition varies significantly at the same temperature and C-rate. We can see that the C-rate above 0.2 is increasing the degradation rate as well as -10ºC compared to +25ºC. This is for both LFP and NMC batteries. It is usually said that LFP should not get that hot as energy per kg is lower, but we saw a very high increase to 65ºC at 40A with four cells in series, with each 20Ah, or C-rate 2. This led to the swelling of the batteries significantly. Concerning DOC/DOD many authors report that this is important, like Shabani et al. (2023), but in absolute numbers, it is not that easy to get a reliable figure.

What we have done with our simulation model is to set some average values on degradation rate and from these estimate parameter values. Adjustment is made for large changes in DOC, temperature, and C-rate. We have made these adjustments for each cycle assuming a full cycle. When the cycle is not full, we assume degradation in SOH is a share of the full cycle.

4. BATTERY DEGRADATION MODEL

The battery degradation will depend on several factors like time, temperature, Depth of Discharge (DOD), Depth of Charge (DoC), number of cycles, and C-rate as well as the calendric time as such. It is of interest to define some key numbers to follow that integrate these different factors.

The algorithm we use for the battery simulation is shown in Table 2 (input data), Table 3 (calculations) and Table 4 (calculations for first 21 timesteps during charging) below.

Table 2. Input data to battery simulator. In this case a single LFP cell.

Input	LFP Cell	Sort
$E_{max,cell}$	64	Wh
$E_{0,cell}$	3.2	Wh
$E_{100,cell}$	60.8	Wh
$U_{max,cell}$	3.7	V
$U_{low,cutoff}$	2.5	V
$U_{0,cell}$	2.5	V
$U_{100,cell}$	3.515	V
$I_{0,cell}$	15	A
$I_{100,cell}$	2	A
U_{normal}	3.2	V
P_{cell}	48	W

The calculations in the simulator are chosen as constant voltage, constant current or constant power. In Table 3 below we see calculations for the constant power case during charging. For discharge the calculation of SoC is slightly different compared to during charging.

Table 3. Calculation for constant power (kW) during charge and discharge

Constant power		
dt	0.016667	h (minute)
$E_{t,cell}$	60.8	$E_{100,cell}$
P_{cell}	48	
$U_{t,cell}$	3.515	$U_{100,cell}$
$I_{t,cell}$	13.65576	$P_{cell}/U_{100,cell}$
$E_{t+1,cell}$	60	$E_{t,cell}-U_{t,cell}*I_{t,cell}*dt$
SoC	0.986111	$(E_{t+1,cell} - E_{0,cell})/(E_{100,cell} - E_{0,cell})$
$U_{t+1,cell}$	3.500903	$U_{t,cell}-(1-SoC)*(U_{100,cell}-U_{0,cell})$
$I_{t+1,cell}$	13.71075	$P_{cell}/U_{t+1,cell}$
Loop	Et,cell=Et+1,cell	
	Ut=Ut+1	
	(It=It+1)	

Principally we calculate an update of SoC for each time step depending on the kW discharge or charge. Calculations are done for a single cell, but several cells in parallel and series are configured to get the correct current, voltage, and energy content (kWh).

Table 4. Calculation of first 10 time-steps during charge of 15 cells in series

Constant power 15 cells										
t	1	2	3	4	5	6	7	8	9	10
dt	0.01667	0.01667	0.01667	0.01667	0.01667	0.01667	0.01667	0.01667	0.01667	0.01667
E_0	48	48	48	48	48	48	48	48	48	48
E_{100}	912	912	912	912	912	912	912	912	912	912
U_0	37.5	37.5	37.5	37.5	37.5	37.5	37.5	37.5	37.5	37.5
U_{100}	52.275	52.275	52.275	52.275	52.275	52.275	52.275	52.275	52.275	52.275
P	720	720	720	720	720	720	720	720	720	720
I_0	15	15	15	15	15	15	15	15	15	15
I_t	19.2	19.09548	18.9921	18.88983	18.78865	18.68856	18.58952	18.49153	18.39457	18.29861
E_t	48	60.0024	72.0048	84.0072	96.0096	108.012	120.0144	132.0168	144.0192	156.0216
U_t	37.5	37.70525	37.9105	38.11575	38.321	38.52625	38.7315	38.93675	39.142	39.34724
E_{t+1}	60.0024	72.0048	84.0072	96.0096	108.012	120.0144	132.0168	144.0192	156.0216	168.024
SoC	0.013892	0.027783	0.041675	0.055567	0.069458	0.08335	0.097242	0.111133	0.125025	0.138917
U_{t+1}	37.70525	37.9105	38.11575	38.321	38.52625	38.7315	38.93675	39.142	39.34724	39.55249
I_{t+1}	19.09548	18.9921	18.88983	18.78865	18.68856	18.58952	18.49153	18.39457	18.29861	18.20366

If we look at the degradation due to different factors, we can see that cycling conditions can be accounted for with a number of adjustment factors or KPIs:

1. DoD/DoC is calculated as SoC_{in} when a cycle starts minus SoC_{out} when we switch from charging to discharging or the opposite. When DoD/DoC is larger than 60% the amount between actual value and 60% is calculated and multiplied by KPI_{doc}.
2. The temperature is assumed normal between 10°C and 30°C, but increased degradation in proportion to temperature difference higher or lower than this. $KPI_{temp} = T_{operational} – (> 30\,^oC \text{ or } <10^oC) * C_{temp.}$
3. Adjustment for C-rate is $KPI_{c\text{-}rate} =$ C-rate^$^{Cc\text{-}rate}$.
4. Calendric time influence KPIcal = number of hours since manufacture of battery * C_{cal}.

Degradation now becomes average degradation when DOD/DOC is <60%, temperature 10-30°C and C-rate < 0.5. We then add degradation rate as add-ons to this average value.

Degradation of SoH equals to:

$$SoH_{deg} = SoH_{average} + (SOC\text{-}60)*KPI_{doc} + (Temp – >30 \text{ or} <10)*KPI_{temp} + C\text{-}rate*KPI_{c\text{-}rate}$$

The $SOH_{average}$ is calculated from the measured values when conditions are stated as above. For fifty cycles we have eight test sets giving an average of 0.045%/cycle. For 325 and 435 cycles we have used two data sets, giving 0.015%/cycle. These are the base values under “normal conditions”. So $SOH_{average,50}$ = 0.045% and $SOH_{average,400}$ = 0.015%. We assume the same for both NMC and LFP batteries.

When the temperature went down to -10°C, the degradation rate for NMC batteries was 1.16%/cycle at C-rate 0.5 and 3.6%/cycle at C-rate one. For C-rate going from 0.5 to 2 the degradation rate went from 0.001 to 0.0079 for LFP battery and from 0.038 to 0.41 for a NMC battery in one set but from 0.07 to 0.05 in another! The tests unfortunately give quite diverse measures! At extreme temperatures we normally see significant degradation of SOH, but sometimes less than expected. We thus have chosen to use conservative values. The plan is to use future measurements to make these factors better by time, including both measurements done in lab as well as including module and pack data from different vehicles. The following values have been set as our initial estimates: KPI_{doc} = 0.002, KPI_{temp} = 0.005, $KPI_{C\text{-}rate}$ = 0.01. This would give for DOD=90, temperature 0°C and C-rate 2 a $SoH_{deg,400}$ = 0.015 + (90-60)*0.002 + 10*0.005 + 2*0.01 = 0.145%.

Battery degradation could be modelled as U=I*R where R is increased as a function of degradation of SoH. The correlation between inner resistance and SoH is that a decrease of R by 0.18 to 0.213Ohm correspond to a decrease in SoH by 8% during three hundred cycles according to Wang et al. (2023). This means 0.027% per cycle. This is a reasonable value if we assume 25°C and C-rate 0.2-0.5. We also assume DOC/DOD to be 60% (SoC 20-80%).

The actual power then could be calculated as $P_{actual} = P*(R_{original}/R_{present})$. When we demand $P = 980W$, we only get $P*(R_{original}/R_{present})$ which is lower than demanded, assuming that total resistance is increasing.

In our simulation model though we are using the SoH degradation depending on temperature, DOC/DOD and C-rate as stated previously. From this we can calculate battery degradation giving RUL and SoH from running with different scenarios with respect to the different conditions.

5. POWER DEMAND FROM VEHICLE

The power demand for each time step is given from a model over e.g. a train line going from one station to the next. There is a time schedule that must be followed given the limitations with respect to acceleration, deceleration, and average

velocity. When passing sensitive areas there are speed limitations e.g. 80 km/h to reduce the impact of noise. The power demand for a train line is seen in Fig. 8 below. The power demand is calculated from the weight of the train, distance, inclination, velocity limitations, acceleration, friction due to bearings, and wind. The results are shown in Fig. 9. The power demand is in kW. Positive values are discharging batteries and negative values charging the batteries due to "motor breaking".

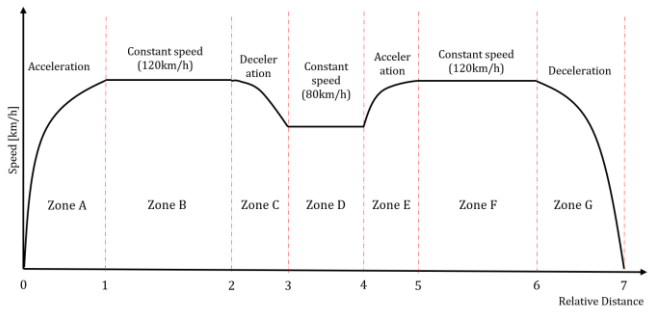

Fig. 8. A train line with seven zones with different conditions with respect to velocity, inclination and acceleration/deceleration.

From the data in Fig. 8 power demand for each zone is calculated and sent to the battery simulator. In Fig. 9 we see the speed of the train in each zone, or more precisely the velocity of the train when it enters and leaves the zone. Thereafter we see the power demand as kW in each zone, the energy output or input to the battery as kWh and finally the state of charge, SoC, calculated for each zone. In this case there were just seven zones, but where there are major accelerations/decelerations each zone may be divided into several zones.

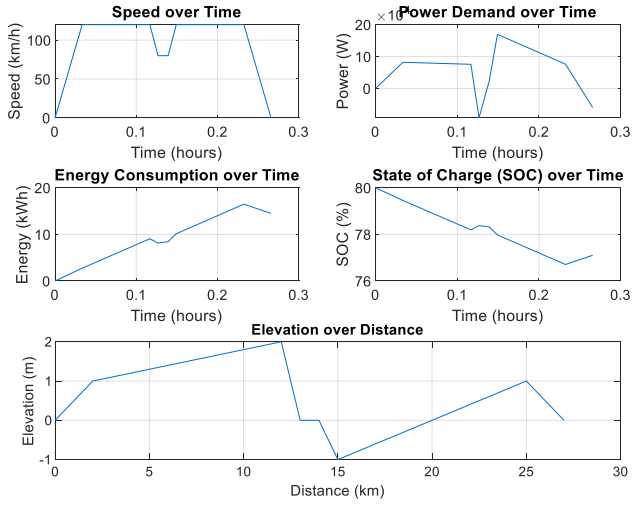

Fig. 9. Speed in km/h in each zone (top), power demand (kW), energy transfer (kWh) and finally state of charge (SoC) in/out of each zone.

For each full cycle, we do a calculation on degradation of SoH due to calendric time, temperature, DOD/DOC and C-rate. For part of a full cycle, that is how much of a full cycle before changing from charging to discharge or vice versa, we do this calculation as percent of a full cycle, so as a function of total Ah stored and used.

6. DISCUSSION AND CONCLUSIONS

From the experimental results, we have made prediction models for RUL and SoH. Concerning the battery simulator, we have formulated the equations for constant power during each section of the distance of a vehicle, or during a certain time period. By running scenarios like a train line as above or some other driving cycle for another type of vehicle, we can simulate future degradation and from this calculate RUL and SoH at certain times, or for "end of life" (EOL). Also calculations can be made on when SoH has reached e.g. 80%, where a second life use would be recommended. From the intensity of the drive cycle, we also can recommend suitable use of the batteries for this second life use. In case of harsh cycles, it may be better to use the batteries for only energy storage like in photovoltaic (PV) cell applications. If low DOD/DOC has been applied generally, a power application, like for example frequency control, can be possible, where high power may be demanded.

ACKNOWLEDGEMENTS

We thank our partner companies, especially Alstom, in the project SITE1, financed by the Swedish Energy Agency aside from Alstom in the grant 2020-021322 (project number 49896-2). We also thank the Knowledge Foundation (KKS) for the support through the SYNERGY project Circul8 (Smart Circular Battery System) with number 20230024.

REFERENCES

Ahmadian, A., Sedghi, M., Elkamel, A., Fowler, M., and Golkar, M.A. (2018). Plug-in electric vehicle batteries degradation modeling for smart grid studies: Review, assessment and conceptual framework. *Renewable and Sustainable Energy Reviews*, 81, 2609–2624.

Chirumalla, K., Kulkov, I., Parida, V., Dahlquist, E., Johansson, G., Stefan, I. (2024). Enabling battery circularity: Unlocking circular business model archetypes and collaboration forms in the electric vehicle battery ecosystem. Technological Forecasting and Social Change, 199, 123044.

Chirumalla, K., Kulkov, I., Vu, Felix., Rahic, M. (2023). Second life use of Li-ion batteries in the heavy-duty vehicle industry: Feasibilities of remanufacturing, repurposing, and reusing approaches. Sustainable Production and consumption, 42, 351-366.

Dahlquist, E., Wallin, F., Chirumalla, K., Toorajipour, R., Johansson, G. (2023). Balancing power in Sweden using different renewable resources, varying prices and storages like batteries in a resilient energy system. Energies, 16(12), 4734

Dai, H., Zhao, G., Lin, M., Wu, J., and Zheng, G. (2018). A novel estimation method for the state of health of lithium-ion battery using prior knowledge-based neural network and markov chain. *IEEE transactions on industrial electronics*, 66(10), 7706–7716.

de la Vega, J., Riba, J.R., and Ortega-Redondo, J.A. (2023). Mathematical modeling of battery degradation based on direct measurements and signal processing methods. *Applied Sciences*, 13(8), 4938.

Gaddipati, G.R. and Kuthuri, N.R. (2023). Enhanced lithium-ion battery model for estimation of degraded capacity and soc using sigma point Kalman filter. *International Journal of Renewable Energy Research (IJRER)*, 13(2), 857–870.

Iurilli, P., Brivio, C., and Wood, V. (2021). On the use of electrochemical impedance spectroscopy to characterize and model the aging phenomena of lithium-ion batteries: a critical review. *Journal of Power Sources*, 505, 229860.

Lam, L. and Bauer, P. (2012). Practical capacity fading model for li-ion battery cells in electric vehicles. *IEEE transactions on power electronics*, 28(12), 5910–5918.

Li, Z., Liu, D., Xiong, J., He, L., Zhao, Z., and Wang, D. (2020). Selective recovery of lithium and iron phosphate/carbon from spent lithium iron phosphate cathode material by anionic membrane slurry electrolysis. *Waste management*, 107, 1–8.

Lin, M., Yan, C., Wang, W., Dong, G., Meng, J., and Wu, J. (2023). A data-driven approach for estimating state-of-health of lithium-ion batteries considering internal resistance. *Energy*, 277, 127675.

Maheshwari, A., Paterakis, N.G., Santarelli, M., and Gibescu, M. (2020). Optimizing the operation of energy storage using a non-linear lithium-ion battery degradation model. *Applied Energy*, 261, 114360.

O'Kane, S.E., Ai, W., Madabattula, G., Alonso-Alvarez, D., Timms, R., Sulzer, V., Edge, J.S., Wu, B., Offer, G.J., and Marinescu, M. (2022). Lithium-ion battery degradation: how to model it. *Physical Chemistry Chemical Physics*, 24(13), 7909–7922.

Panchal, S., Mcgrory, J., Kong, J., Fraser, R., Fowler, M., Dincer, I., and Agelin-Chaab, M. (2017). Cycling degradation testing and analysis of a lifepo4 battery at actual conditions. *International Journal of Energy Research*, 41(15), 2565–2575.

Pelletier, S., Jabali, O., Laporte, G., and Veneroni, M. (2017). Battery degradation and behaviour for electric vehicles: Review and numerical analyses of several models. *Transportation Research Part B: Methodological*, 103, 158–187.

Qadrdan, M., Jenkins, N., and Wu, J. (2018). Smart grid and energy storage. In *McEvoy's Handbook of Photovoltaics*, 915–928. Elsevier.

Rahbari, O., Mayet, C., Omar, N., and Van Mierlo, J. (2018). Battery aging prediction using input-time- delayed based on an adaptive neuro-fuzzy inference system and a group method of data handling techniques. *Applied Sciences*, 8(8), 1301.

G. Geetha Ravali* , K. Narasimha Raju: Enhanced Lithium-Ion Battery Model for estimation of Degraded Capacity and SoC Using Sigma Point Kalman Filter. International journal of renewable energy research, Vol.13, No.2, June, 2023

Rojas Vazquez Josefin: Battery capacity prediction using deep learning. Master thesis work,Malardalen University press, 2023.

Salazar, E. and Bengoechea, J. (2021). Research paper lithium and its role in the new energy transition. *Bachelor Thesis, Geneva Business School*.

Shabani, M., Wallin, F., Dahlquist, E., and Yan, J. (2023). The impact of battery operating management strategies on life cycle cost assessment in real power market for a grid-connected residential battery application. *Energy*, 270, 126829.

Shamarova, N., Suslov, K., Ilyushin, P., and Shushpanov, I. (2022). Review of battery energy storage systems modeling in microgrids with renewables considering battery degradation. *Energies*, 15(19), 6967.

Shen, D., Xu, T., Wu, L., and Guan, Y. (2019). Research on degradation modeling and life prediction method of lithium-ion battery in dynamic environment. *IEEE Access*, 7, 130638–130649.

Shi, E., Xia, F., Peng, D., Li, L., Wang, X., and Yu, B. (2019). State-of-health estimation for lithium battery in electric vehicles based on improved unscented particle filter. *Journal of Renewable and Sustainable Energy*, 11(2).

Uddin, K., Perera, S., Widanage, W.D., Somerville, L., and Marco, J. (2016). Characterising lithium-ion battery degradation through the identification and tracking of electrochemical battery model parameters. *Batteries*, 2(2), 13.

Wang, Z., Zhao, X., Fu, L., Zhen, D., Gu, F., and Ball, A.D. (2023). A review on rapid state of health estimation of lithium-ion batteries in electric vehicles. *Sustainable Energy Technologies and Assessments*, 60, 103457.

Wildfeuer, L., Karger, A., Aygül, D., Wassiliadis, N., ossen, A., and Lienkamp, M. (2023). Experimental degradation study of a commercial lithium-ion battery. *Journal of Power Sources*, 560, 232498.

Xiong, R., Huang, J., Duan, Y., and Shen, W. (2022). Enhanced lithium-ion battery model considering critical surface charge behavior. *Applied Energy*, 314, 118915.

Zhang, X., Sun, P., Wang, S., and Zhu, Y. (2023).
Experimental study of the degradation characteristics of lifepo4 and lini0. 5co0. 2mn0. 3o2 batteries during over-charging at low temperatures. *Energies*, 16(6), 2786.